Variation of the Eddy Diffusivity Across Jets in the Southern Ocean

by:

Ali Mashayek

Supervisors:

Oliver Bühler & Raffaele Ferrari

August 2009

1 Introduction

Large scale ocean circulation is one of the main components of the climate system. The enormous heat capacity of the oceans makes general oceanic circulation a great means of transport of considerable amount tracers such as heat across the globe. Thus, a growing number of research activities have been focused on understanding the oceans as a part of the climate system. The main goal is to develop tools that will enable scientists to understand the past history of the climate system and more importantly, to make predictions about the future. The complexities of the components of the climate system such as the oceans and the atmosphere demand numerical models to simulate their behaviors in conditions close to reality. In particular, ocean general circulation models (GCM) have been developed with the aim of simulating the general circulation and more local characteristics of the ocean. The current ocean models used for climate studies cannot resolve the fine scale turbulence and eddy characteristics due to computational cost limitations. Thus, resorting to parameterizations for fine scale behaviors is inevitable. One of the key parameters used in the GCMs to capture the turbulent characteristics is the eddy diffusivity, K, which relates the flux of tracers to their mean gradients. This parametrizaion however requires proper knowledge of the magnitude and variations of K as a function of latitude-longitude and depth as well as its temporal variations. Great effort has been devoted to enhancing our knowledge of the diffusivity over the past years. As one particular case, estimating the tracer transport across a permanent jet is of great importance. The transport of heat across the Antarctic Circumpolar Current (ACC) for example is of great importance specially in the context of global warming and melting of the land ice sheets located in the Antarctica. Ferrari and Nikurashin (2009) [1] (hereafter referred to as FN09) studied the variations in the eddy diffusivity across the jets in the southern ocean. They compared different methods of measurement of the the diffusivity and investigated the effect of the eddy-mean flow interaction on the diffusivity across the jet. Several studies (such as those listed in FN09) have used the mixing length theory to relate the diffusivity to the r.m.s velocity of the eddies and the mixing length l. The mixing length was often set proportional to the observed eddy sizes. This method led to a peak in the values of K in the core of the ACC due to larger eddy velocities. A different approach taken by Marshal *et al.*(2006) [3] provided estimates of the diffusivity by feeding flow simulations by velocities obtained from observation and studying the diffusion of an artificially (numerically) injected passive tracer field into the domain. They suggested that the diffusivity is rather suppressed in the core of the ACC and enhanced in its flanks as opposed to the first group of studies. FN09 explained this discrepancy by pointing out that the mixing length used in the first class of studies is not necessarily of the same order of the eddy sizes. Using a dynamic model, FN09 showed that the mixing length is modulated by the mean flow and the relative velocity between the main flow and the speed of travelling of the eddies reduces the diffusivity. Thus, the large values of K found by the earlier studies was mainly due to not taking the reduction of the mixing length into account. It should also be mentioned that Marshal *et al.*(2006) speculated that the large values of K in the flank of the ACC can be due to the presence of critical layers.

Since our motivation for the present work is based on the model proposed by FN09, a brief introduction to their model is necessary before the motivation of our work can be

explained. Starting from a uniform zonal flow of constant velocity U_0, FN09 applied the surface Quasi-Geostrophic (QG) formulation to describe the dynamics and used it to derive an expression for the eddy diffusivity. The governing equations they started from are

$$b_t + J(\psi - U_0 y, b - \Gamma y) = 0, \tag{1}$$

$$\partial_x^2 \psi + \partial_y^2 \psi + \frac{f^2}{N^2} \partial_z^2 \psi = 0, \tag{2}$$

where ψ is the perturbation (from the mean) geostrophic stream function, b is the perturbation surface buoyancy, J is the Jacobian operator, Γ is the constant lateral gradient of the background buoyancy $\partial_y B = -\Gamma$, and f and N are the inertial and stratification frequencies respectively. They expanded (1) to get

$$\partial_t b + U_0 \partial_x b - \Gamma \psi_x = fN\sqrt{\gamma} r(t) e^{i(kx+ly)} - \gamma b, \tag{3}$$

where the nonlinear term $J(\psi, b)$ in (1) is expressed in the form of a fluctuation-dissipation stochastic model which is a crude representation of excitation of waves by baroclinic instability at the most unstable wave number (k, l). The model is in terms of a stochastic variable $r(t)$ and a linear damping rate γ. The variable $r(t)$ is a white-noise function with the property $< r(t) r(t')^* >= \delta(t - t')$ where '$< >$' denotes the "expected value". The stochastic forcing "mimics the nonlinear damping of each wave through interaction with other waves"[1]. The constant f sets the forcing amplitude. The forcing is kept monochromatic to keep the problem linear. FN09 showed that this model generates a velocity field with a correlation function decaying exponentially at the rate γ. The solution of the stream function was obtained from (1,2) in the form of

$$\psi = \frac{f}{\kappa}\sqrt{\gamma} \int_0^\infty r(t-\tau) e^{i(kx+ly-kc_w\tau)-\gamma\tau+\frac{N\kappa}{f}z} d\tau, \tag{4}$$

where $\kappa^2 = k^2 + l^2$, $\kappa_d^{-1} = \frac{NH}{f}$ is the deformation radius, and $c_w = (1 - \frac{\kappa_d}{\kappa})U_0$ is the phase speed of the surface waves embedded in the current U. Next they considered a tracer S with a constant gradient $\Gamma_s = \frac{dS}{dy}$ embedded in the eddy field (4) given by

$$S_t + J(\psi - U_0 y, S) = -\Gamma_s \partial_x \psi. \tag{5}$$

After solving for S from the above equation, and obtaining the jet cross-stream velocity v from the stream function in (4), they calculated the tracer flux across the jet to be

$$< vS >= -[\frac{1}{2} f^2 \frac{k^2}{\kappa^2} \frac{\gamma}{\gamma^2 + k^2(c_w - U_0)^2} e^{2\frac{N\kappa}{f}z}]\Gamma_s. \tag{6}$$

The eddy diffusivity $K_\perp$ can be obtained by dividing (6) by Γ_s. The simple expression (6) has an important physical interpretation. It shows that for an eddy phase speed equal to the jet mean velocity U_0, the eddy diffusivity has a maximum value and indeed yields a value similar to those obtained by the group of studies which used the mixing length to relate the observations to the diffusivity. However, as the relative velocity of the eddies to the main current increases, the denominator of (6) becomes larger leading to a suppression in the diffusivity. In practice, this relative velocity is large (about 13 cm/s for the ACC)

and comparable to the main jet speed U_0 (which is about 15 cm/s in the core of the ACC). Thus, the suppression effect is pronounced in the core of the ACC as shown by Marshal *et al.*(2006) [3]. Neglecting the $(c_w - U)^2$ in the denominator of (6) leads to overestimation of the mixing length and thus, over prediction of the diffusivity. It should also be noted that the suppression is strong if the decorrelation timescale of the eddy is much slower than the advection of the tracer out of the eddy due to the relative velocity (i.e. if $k^2(c_w - U)^2 \gg \gamma^2$).

The FN09 expression for tracer flux mentioned above is for an ideal environment of infinite extent and with a constant velocity and constant stochastic forcing over the whole domain. Left panel of figure 1 shows the zonally averaged eddy kinetic energy and mean jet velocity curves for a patch of the southern ocean between 125^oW-150^oW and 66^oS-30^oS. The right panel of the figure shows a snapshot of the observed sea surface height anomalies for the same patch. As the figures show, there is considerable variations in both the forcing (eddy field) and the jet velocity from the main core of the ACC to its flanks. Thus, one can curiously wonder what happens if continuous or piece-wise continuous variations in the forcing and jet velocity are considered in the context of the model developed by FN09. To be more clear, the question is whether (and how) the expression (6) would change if for example we considered two semi-infinite velocity zones of adjacent flows with different forcing or different velocities? The main motivation of this study is to take the model explained above few steps further by allowing for these variations and investigating their effects on the tracer fluxes. In what follows in the remainder of this article, we start from a simple case of two semi-infinite adjacent zones and allow for variations in the forcing and the velocities between the two zones. The approach is to start from the simplest case and add complexity to the problem step by step to gain insight into the basic physics of the problem.

2 Barotropic Quasi-Geostrophic Formulation

As mentioned by FN09, their final results on eddy mixing are independent of their particular choice of the surface Quasi Geostrophic (QG) model. We opt to use two-dimensional barotropic QG formulations in this work and will recover the FN09 results for the surface of the ocean ($z = 0$). Modifying the formulation and results of this work to the surface QG formulation is an easy and straight forward task and only adds an exponential z-dependence to the stream functions and the fluxes obtained. Starting from 2D barotropic QG equations we have

$$q_t + J(\psi, q) = 0, \tag{7}$$

$$\nabla^2\psi - \kappa_D^2\psi = q - \beta y, \tag{8}$$

where q is the potential vorticity, $\kappa_D^{-1} = \sqrt{gH_0}/f_0$ is the deformation radius, and ψ is the velocity stream function. In the QG formulation, $\psi = \frac{g\eta}{f_0}$ where η is the surface elevation (or depression) from the reference surface level (located at H_0 above the flat bottom boundary). Since η is easily related to the pressure, the stream function can be interpreted as the surface pressure or the surface height and thus, can be estimated from altimetry data. In the two above formulae and all that follows beyond this point, a subscript denotes a differentiation. Next we make the assumption that the potential vorticity, q, is a function of the meridional

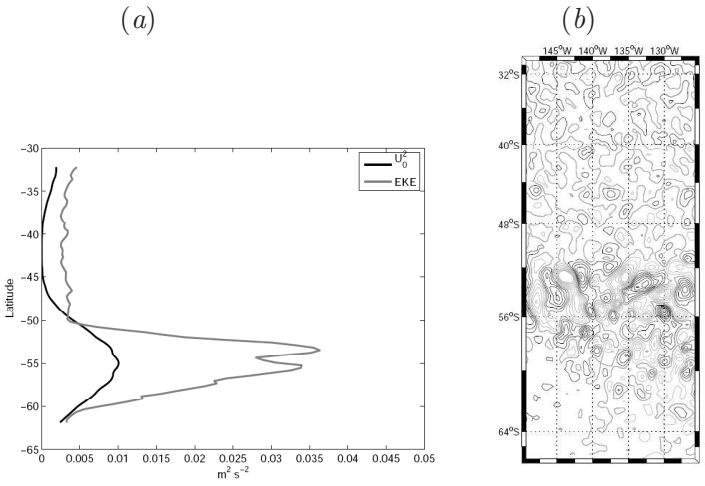

Figure 1: (*a*)Zonally averaged mean kinetic energy (black) and eddy kinetic energy (EKE) (gray) at the surface for a patch in the Pacific sector of the Southern Ocean between 125W-150W and 66S-30S; (*b*) Snapshot of sea surface height anomaly for the same patch: (black) positive anomaly, (gray) negative anomaly. (Taken from Ferrari and Nikurashin 2009 by permission).

coordinate y alone and so $q = Q(y)$. This assumption along with (8) mean that ψ is also only a function of y and so $u = -\psi_y = U(y)$ and $v = \psi_x = 0$. The equation (8) takes the simpler form

$$\frac{d^2\psi}{dy^2} - \kappa_D^2\psi = Q(y) - \beta y. \tag{9}$$

Next we perturb equations (7,8) around a mean flow $u = U(y)$ by introducing

$$\begin{aligned} q &= Q + \epsilon q', \\ \psi &= \Psi + \epsilon\psi', \\ u &= U + \epsilon u', \\ v &= \epsilon v'. \end{aligned} \tag{10}$$

Substituting (10) into (7,8) we get

$$q_t + \frac{1}{\epsilon}Q_t + J(\Psi, q') + J(\psi', Q) + \frac{1}{\epsilon}J(\Psi, Q) + \epsilon J(\psi', q') = 0, \tag{11}$$

$$(\nabla^2 - \kappa_D^2)\psi' = q'. \tag{12}$$

The second and the fifth term in (11) form the background field and sum up to zero. The $J(\Psi, q')$ term simplifies to $U(y)a'_x$ and the $J(\psi', Q)$ simplifies to $Q(y)\psi'_x$ leading to

$$(\partial_t + U\partial_x)q' + Q_y\psi'_x = \mathcal{F} \tag{13}$$

where $\mathcal{F}$ is the nonlinear term coming from $J(\psi', q')$. Dropping the primes we reach the linearized QG equations for the perturbation quantities q and ψ:

$$(\nabla^2 - \kappa_D^2)\psi = q, \tag{14}$$

$$(\partial_t + U(y)\partial_x)q + Q_y\psi_x = \mathcal{F}. \tag{15}$$

The Q_y term can be obtained by taking the y-derivative of (9)

$$Q_y = \beta + \kappa_D^2 U(y) - U(y)_{yy}. \tag{16}$$

The set of equations (14,15) will be the starting point of our analysis in the consequent sections. As we will see, the background velocity $U(y)$ is considered to be constant (or piecewise constant) throughout this article and thus the third term in (16) drops out and the second term simplifies to a constant value.

3 Basic Case: Non-stochastic forcing

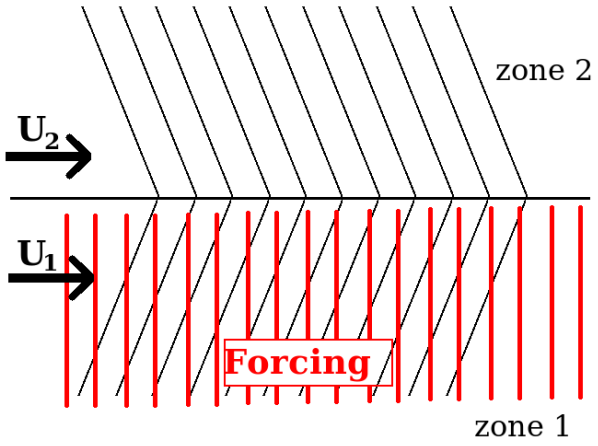

Figure 2: Schematic view of the basic case flow configuration.

As the first basic case, we consider two semi-infinite adjacent zones with velocities U_1 and U_2. Figure 2 shows the schematic of the problem. The top zone (zone 2) is an unforced region while the bottom zone is forced with a monochromatic forcing in the form of:

$$\mathcal{F} = fe^{ik(x-ct)}, \tag{17}$$

where f is the forcing amplitude, k is its x-direction wavenumber and c is the corresponding phase speed. The forcing is chosen to be monochromatic to keep the problem linear. Although a y-dependence can also be included in the expression for forcing, it does not add new physics into the problem and (17) can be used without loss of generality. The forcing is demonstrated by the red vertical lines in the figure. The linearized form of the governing equations in the top layer takes the form

$$(\nabla^2 - \kappa_d)\psi = q_2 \tag{18}$$

$$(\partial_t + U\partial_x)q_2 + \beta\psi_{2,x} + \gamma q_2 = 0, \tag{19}$$

and in the bottom layer we have

$$(\nabla^2 - \kappa_d)\psi = q_1 \tag{20}$$

$$(\partial_t + U\partial_x)q_1 + \beta\psi_{1,x} + \gamma q_1 = \mathcal{F}. \tag{21}$$

It is easy to see that the solution of (19) and the homogeneous solution of(21) have the general form:

$$\psi = ae^{ily} + be^{-ily}, \tag{22}$$

where a and b are constants and l is

$$l = \sqrt{\frac{\Gamma}{U-c} - (k^2 + \kappa_D^2)}, \tag{23}$$

where $\kappa_D^{-1} = \sqrt{gH_0}/f_0$ is the deformation radius for the barotropic case and $\Gamma = \beta + \kappa_D^2 U$ is a constant. We consider homogeneous solutions that radiate out from the interface and pick the proper term of (22) for each zone. Next, we set to calculate the particular solution of (21). To do that, we notice that the following expressions for ψ and q satisfy (21):

$$\psi = -A\frac{f}{k^2 + \kappa_D^2}\, e^{ik(x-ct)}, \tag{24}$$

$$q = Af\, e^{ik(x-ct)}. \tag{25}$$

Replacing these into (21), the coefficient A becomes

$$A = \frac{1}{\gamma + ik(U_1 - c - \frac{\Gamma}{k^2+\kappa_D^2})}. \tag{26}$$

It should be noted that A is an imaginary number and would be pure imaginary in the absence of the damping coefficient, γ. So, the total solution in the two zones become

$$\psi_1 = [a_1 e^{-il_1 y} - A\frac{f}{k^2 + \kappa_D^2}]e^{ik(x-ct)}, \tag{27}$$

$$\psi_2 = a_2 e^{il_2 y} e^{ik(x-ct)}. \tag{28}$$

Coefficients a_1 and a_2 can be found by matching the interfaces using two jump conditions which are originally due to Rayleigh (1880) [4]. The first jump condition ensure that the stream function (which can be interpreted as surface height in the QG formulation) is continuous across the interface. The second jump condition is that the displacement of the interface between the two regions of the flow be the same on both sides of the interface to ensure no cavitation occurs. A general derivation of these two conditions will be presented in the next section. For this case however, these conditions simply take the form

$$\Delta(\frac{\psi}{U-c}) = 0, \tag{29}$$

$$\Delta(\psi_y(U-c)) = 0, \tag{30}$$

were Δ stands for jump across the interface and both conditions are enforced at $y = 0$. Applying these conditions to the two stream functions we get

$$a_1 = \frac{ABl_2}{R^2 l_1 + l_2}, \tag{31}$$

$$a_2 = -\frac{ABRl_1}{R^2 l_1 + l_2}, \tag{32}$$

where $R = \frac{U_1 - c}{U_2 - c}$ and $B = \frac{f}{k^2 + \kappa^2}$. Next we set to calculate the cross-jets diffusivities in the two zones. Following FN09, we introduce the equation for the transport of a passive scalar in the fields described by stream functions (27, 28):

$$S_t = -J(\psi_i - U_i y, S - \Gamma_s y), \tag{33}$$

where Γ_s is a constant background tracer gradient equal to $\frac{d_B}{dy}$ and $i = 1, 2$ corresponds to the two zones. Rearranging we get

$$S_t + J(\psi, S) + U_i S_x = -\Gamma_s (\psi_x)_i = -\Gamma_s v_i. \tag{34}$$

We will shortly see that the second term in (34) is zero and the scalar equation reduces to

$$S_t + U_i S_x = -\Gamma_s v_i. \tag{35}$$

Solving (35) for the two zones using (27,28), the solutions of the scalar fields becomes:

$$S_1 = \frac{-\Gamma_s}{U_1 - c}(a_1 e^{-il_1 y} - AB)e^{ik(x-ct)}, \tag{36}$$

$$S_2 = \frac{-\Gamma_s}{U_2 - c}(a_2 e^{-il_2 y} - AB)e^{ik(x-ct)}. \tag{37}$$

One can substitute (36, 37) back into the $J(\psi, S)$ in (34) to confirm that the Jacobian vanishes. With the solutions of the scalar field obtained in both zones, we can calculate the diffusivity

$$K_\perp = \frac{1}{\Gamma_s} \Re < Sv >. \tag{38}$$

According to (36) for the first zone we have

$$S_1 = \frac{\Gamma_s}{ik(U_1 - c)}, \tag{39}$$

and thus the cross-jet flux becomes

$$\Re < Sv > = \frac{k(U_1 - c)}{\Gamma_s} \Re < iS_1 S_1 > = 0. \tag{40}$$

This simply means that for a velocity field of the general form $v = \cos(\alpha) + i \sin(\alpha)$, the solution to the scalar equation takes the form $S = c - \sin(\alpha) + i \cos(\alpha)$ and so the flux $\Re < Sv >$ takes the form $< \sin(\alpha) \cos(\alpha) >$ which is identically zero. Repeating the analysis

for the second zone yields the same result. This outcome simply indicates that a linear monochromatic forcing (which yields to north and south monochromatic radiations) cannot mix the fluid. To introduce diffusion (i.e., a nonzero flux) one has to either take into effect the nonlinear wave dynamics and wave interactions or introduce a forcing (and the consequent radiations) that decorelate from itself in a finite time. The second approach was that taken by FN09. In the next section we introduce a random forcing to investigate its effects. But before that, an interesting point can be observed by a closer look at equations (36, 37, 40). If the velocity of the main flow in one of the zones (lets say U_1) is equal to the zonal phase speed of the wave propagation, then the conclusion obtained above is not strictly valid. To better understand this fact, one can assume a single one-dimensional wave propagating eastward in the absence of any mean flow. The streamlines of the flow inside the fluid induced by the wave propagation form closed circulating regions and particle paths form closed elliptic curves. So, a particle (or a tracer filament) departing from some arbitrary initial location will return to its initial location due to the linear wave propagation. An introduction of any nonlinear effect (such as the Stoke's drift) will lead to the particle not returning to its initial position and thus mixing. This is also true for the case were a uniform background velocity U is superposed as one can go to the reference frame moving with U and observe the wave with the relative phase speed $U-c$. However, if the wave phase speed and the background flow velocities are the same (i.e., $U-c=0$), then an observer sitting on the reference frame which moves with U will observe a frozen wave pattern with fixed recirculating regions (a critical layer). Particles or tracer filaments left in these regions will mix with the ambient fluid at a high rate and considerable mixing will occur. That is why the value of the flux in equation (40) can not be clearly estimated in this limit as the denominator tends to zero. This behavior will be further examined in the next section.

4 Case I: Semi-infinite white-noise forcing

As the first case with random forcing, we consider two semi-infinite adjacent zones with similar velocities U. Figure 3 shows the schematic of the problem. The top zone (zone 2) is an unforced region while the bottom zone is forced similar to the previous section but with a stochastic forcing in the form of:

$$\mathcal{F} = f\kappa\sqrt{\gamma}\, r(t) e^{ikx} - \gamma q, \tag{41}$$

where f is the forcing amplitude, and $r(t)$ is a stochastic stationary variable satisfying $< r(t)r^*(t') >= \delta(t-t')$. The forcing is chosen to be monochromatic to keep the problem linear and is a crude representation of the wave excitation by the baroclinic instability and thus, k can be interpreted as the wave number of the most unstable mode of the instability.

The linearized form of the governing equations in the top layer takes the form

$$(\nabla^2 - \kappa_d)\psi = q_2 \tag{42}$$

$$(\partial_t + U\partial_x)q_2 + \beta\psi_{2,x} + \gamma q_2 = 0, \tag{43}$$

and in the bottom layer we have

$$(\nabla^2 - \kappa_d)\psi = q_1 \tag{44}$$

$$(\partial_t + U\partial_x)q_1 + \beta\psi_{1,x} + \gamma q_1 = \mathcal{F}. \tag{45}$$

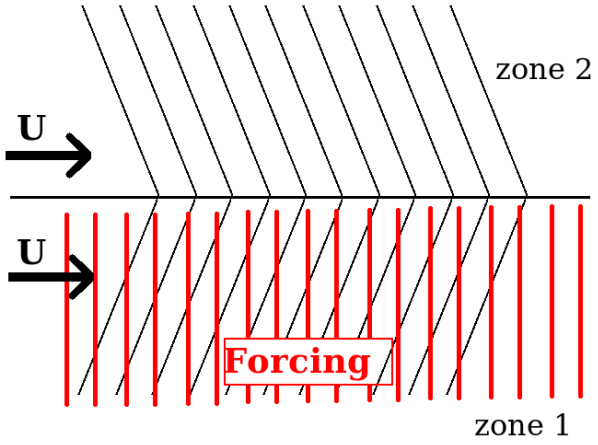

Figure 3: Schematic view of the case I flow configuration.

From previous section we know that the homogeneous solutions of equations (43, 45) can be written in the form of

$$\psi_h = e^{ikx} \int A(\omega)\, e^{il(\omega)y}\, e^{i\omega t} d\omega, \tag{46}$$

Substitution of (46) in (43) and in the homogeneous part of (45) leads to the dispersion relation

$$\omega = Uk + i\gamma - \frac{\beta k}{l^2 + k^2 + \kappa_d^2}. \tag{47}$$

Using 47 one can calculate the vertical wavenumber l for any particular frequency ω. However, the choice of l in zone 2 should be made in the way that all wave components travel away from the interface (and thus $\Re(l_2) > 0$) and all components decay as $y \to \infty$ (and thus $\Im(l_2) > 0$). A single component of such form is shown in zone 2 in figure 3 as the representative of the homogeneous solution in that zone. The components of the homogeneous solution in zone 1 should also travel downward and decay as $y \to -\infty$. This translates to $l_1(\omega) = -l_2(\omega)$. A single component of such form is also shown in zone 1 in the figure in black. We next set to derive the particular solution of the forced equation (45). To do that, we note that

$$q_{p1} = -a(t)\kappa f e^{ikx}, \qquad \psi_{p1} = a(t)\frac{f}{\kappa} e^{ikx} \tag{48}$$

satisfy the equations (44, 45). Substitution of (48) into (45) gives

$$a_t + [\gamma + ik(U - \frac{\beta}{\kappa^2})]a = \sqrt{\gamma} r(t), \tag{49}$$

which can be solved to give

$$a(t) = \sqrt{\gamma} \int_0^\infty e^{-(\gamma + ikc_w)\tau}\, r(t-\tau) d\tau, \tag{50}$$

where $c_w = U - \frac{\beta}{\kappa^2}$ is the phase speed of the eddies embedded in the current U. Thus the particular solution in zone 1 takes the form

$$\psi_{p1} = \frac{f}{\kappa}\sqrt{\gamma}\; e^{ikx} \int_0^\infty e^{-(\gamma + ikc_w)\tau}\; r(t-\tau)d\tau, \tag{51}$$

and the total solutions in the two zones become

$$\psi_2 = \psi_{h2} = e^{ikx} \int A_2(\omega)\; e^{il(\omega)y}\; e^{i\omega t} d\omega, \tag{52}$$

$$\psi_1 = \psi_{h1} + \psi_{p1} = e^{ikx} \int A_1(\omega)\; e^{-il(\omega)y}\; e^{i\omega t} d\omega + \frac{f}{\kappa}\sqrt{\gamma}\; e^{ikx} \int_0^\infty e^{-(\gamma + ikc_w)\tau}\; r(t-\tau)d\tau. \tag{53}$$

The stream functions (52 and 53) have to satisfy the jump conditions across the interface. The fist jump condition can be obtained by integrating the stream functions across the interface:

$$\int_{-\epsilon}^{0} \psi_1\; dy = \int_0^{+\epsilon} \psi_2\; dy. \tag{54}$$

Calculating the limit of (54) as $\epsilon \to 0$ gives the fist jump condition at the interface

$$A_1(\omega) = -A_2(\omega). \tag{55}$$

The second jump condition can be obtained by requiring the solution for the interface perturbation η (shown schematically in figure 11) obtained in the two zones to be equal to each other. Using (101) from appendix **A** and evaluating the jump condition at $y = 0$ we get

$$\hat{A_1} = \frac{1}{2}\hat{\psi_{p1}}, \tag{56}$$

where ' $\hat{}$ ' denotes the Fourier transform. Using (55, 56) and taking the Fourier transform of ψ_{p1} in (51) we get

$$\hat{A_1} = \frac{f}{2\kappa}\frac{\sqrt{\gamma}\; e^{ikx}}{\gamma + i(\omega - kc_w)}\hat{r}(\omega), \tag{57}$$

$$\hat{A_2} = -\frac{f}{2\kappa}\frac{\sqrt{\gamma}\; e^{ikx}}{\gamma + i(\omega - kc_w)}\hat{r}(\omega). \tag{58}$$

Next we set to calculate the $< vS >$ flux for the unforced region (zone 2). As before, the flux equation is

$$(\partial_t + ikU)S = -ik\Gamma\psi \tag{59}$$

multiplying both sides by e^{ikUt} and rearranging we get

$$\tilde{S_t} = -ik\Gamma e^{ikUt}\psi = H(t), \tag{60}$$

where $\tilde{S} = e^{iKUt}S$. As before, the flux can be written in the form

$$< Sv >= \frac{1}{2} < S^*v + Sv^* > . \tag{61}$$

We can write

$$< S^*v >=< S^*(-ik\psi) >=< e^{-iUkt}S^*(-ik\psi)e^{iUkt} >=< \tilde{S}^*\frac{H(t)}{\Gamma} > \tag{62}$$

and according to (60) we get

$$< S^*v >= \frac{< \tilde{S}^*H(t) >}{\Gamma} = \frac{1}{2\Gamma}\frac{d}{dt} < \tilde{S}_t^* > . \tag{63}$$

It is shown in the appendix B that for any two functions $V(t)$ and $S(t)$ if we have $V(t) = bA(t) * r(t)$ and $S_t = V(t)$ (where b is a constant), then $< SV >= \frac{1}{2}\frac{d}{dt} < S^2 >= \frac{1}{2}|bb^*||\hat{A}(0)\hat{A}^*(0)|$.

Thus if we can show that $H(t)$ can be written in the form of $H(t) = bA(t) * r(t)$ then from (63) and (60) we get

$$< S^*v >= \frac{1}{2\Gamma}|\hat{H}(0)|^2 = \frac{1}{2\Gamma}|\hat{H}(0)||\hat{H}^*(0)|. \tag{64}$$

Its easy to show that $< Sv^* >$ has also the same value as $< S^*v >$ and so $< Sv >=< S^*v >$ according to (61). In order to calculate the flux we have to calculate $\hat{H}(0)$ and also show that $H(t)$ has the $bA(t) * r(t)$ form. From (60) we have

$$\hat{H}(\omega) = -ik\Gamma\hat{\psi}(\omega - Uk). \tag{65}$$

Taking the Fourier transform of (52,53) and using (56,57,58) we get

$$\hat{\psi_1} = [\hat{A}_1(e^{-il(\omega)y} + 2)]e^{ikx} = \frac{f}{2\kappa}\frac{\sqrt{\gamma}\, e^{ikx}}{\gamma + i(\omega - kc_w)}\hat{r}(\omega)(e^{-il(\omega)y} + 2)e^{ikx}, \tag{66}$$

$$\hat{\psi_2} = \hat{A}_2 e^{il(\omega)y}e^{ikx} = \frac{f}{2\kappa}\frac{\sqrt{\gamma}\, e^{ikx}}{\gamma + i(\omega - kc_w)}\hat{r}(\omega)e^{il(\omega)y}e^{ikx}, \tag{67}$$

and so both ψ_1 and ψ_2 (and thus H) have the desired $bA(t) * r(t)$ (or $b\hat{A}\hat{r}$) form. It should be noted that in calculating the Fourier transform of ψ_p, we have assumed a non-zero value for the damping rate γ. Thus, in interpreting the results that follow, $\gamma = 0$ is not permitted event hough some equations might suggest it has a meaning. So, according to appendix B and (64), the diffusivity in the forced zone becomes

$$K_1 = \frac{1}{2}|\hat{A}_1\hat{A}_1^*||1 - \frac{e^{-il(\omega)y}}{2}|^2 = \frac{1}{8}\frac{f^2k^2}{\kappa^2}\frac{\gamma}{\gamma^2 + k^2(U - c_w)^2}\,(4 + e^{2\Im(l)y} - 4e^{\Im(l)y}\cos(\Im(l)y)), \tag{68}$$

and in the unforced zone we get

$$K_2 = \frac{1}{8}\frac{f^2k^2}{\kappa^2}\frac{\gamma}{\gamma^2 + k^2(U - c_w)^2}\, e^{-2\Im(l)y} \tag{69}$$

Two interesting points immediately emerge by looking at the expression for K_2. First, the magnitude of the diffusivity at the interface is a quarter of that of the diffusivity of the one infinite zone problem studied by FN09. This could already be known by the second jump condition (56) and noting that $K \propto |\hat{A(0)}|^2$. The second point is the y-dependence of the result in (69). As we move away from the interface in the unforced region, the diffusivity decays exponentially to zero. So the mere introduction of a jump in the forcing leads to differences in magnitude and behavior of the diffusivity in the unforced region.

Expression (68) shows that similar to K_2, K_1 also takes the value of one quarter of that of the infinite-domain case at the interface ($y = 0$) and so the solutions in the two zones match at the interface as expected. However, as $y \to -\infty$, the diffusivity tends to the result obtained in the infinite-domain case. So in the forced region, there is a transition from the value of one quarter of the constant infinite-domain flux at the interface to the full value in the far distances from the interface. This transition however, does not have an exponential decay pattern such as zone 2 and shows oscillatory behavior as determined by the terms in the parenthesis on the right hand side of (68). To demonstrate these behaviors better, figure 4 shows a series of plots of the wave patterns and diffusivity variations in the neighborhood of the interface for a set of parameters. The left column shows the wave pattern for the intrinsic ($\omega - Uk = 0$) wave pattern in the two zones and the right column shows the corresponding diffusivity curves. The relative magnitude of the ratio of the imaginary part of the vertical wave number l (which determines the decay rate in both zones) to the real part of l (which determines the oscillations in the forced zone) changes from 0 in case (a) to 1 in case (e). The green lines in the right column represent the constant diffusivity corresponding to the one-zone problem for the same parameters of each case. Starting from panel (a) where $\Im(l) = 0$, we can clearly see pure oscillatory behavior in both zones. The left panel shows the north-east propagation of waves coming from the homogeneous solution in the upper zone and superposition of a south-east propagation wave(coming from the homogeneous solution in zone 1) and a east propagating wave (coming from the particular solution in zone 1) in the lower zone. These results were expected from the $\omega - Uk = 0$ mode of the solutions (52, 53) in the Fourier space. The right panel shows the corresponding effective diffusivity. Pure oscillatory motion due to the absence of an imaginary part to l is clear as the diffusivity oscillates around the infinite-zone value (green line). It should be noted that as mentioned earlier, the value of the diffusivity at the interface (the point of meeting of the red and blue curves) is one fourth of that of the green line. This value retains a constant value in the unforced zone indicating a constant diffusivity. It is important to note that the $\Im(l) = 0$ condition can be achieved only when $\gamma = 0$ which means in the absence of any damping. Since the assumption of $\gamma \neq 0$ was used in the derivation of (69, 68), case (a) should be treated as a limiting case where $\gamma \to 0$.

As $\Im(l)$ grows larger than zero, the decay in the vertical direction leads to exponential decay of this one-fourth value to zero away from the interface in the upper zone and an oscillatory decay to the green line value in the forced zone. This can be seen as $\Im(l)$ grows to 0.1 in the case (b). The left panel in case (b) also show the decay of the waves to zero as we move away from the interface in the north zone and the decay of the radiative waves in the lower zone until only the forcing pattern remains. As the $\Im(l)/\Re(l)$ ratio increases in cases (c-e), the decaying layer in each zone becomes compressed about the interface. For the final case with $\Im(l)/\Re(l) = 1$, we almost have two regions of constant diffusivity with

a value of zero in the upper zone and that of the one-zone problem in the lower region. Although K still has the one-fourth value (of the green line) at the interface, the transition to the two limiting constant values in the two regions is very fast and limited to the close vicinity of the interface.

It would now be interesting to see how the real physical case corresponding to the ACC would compare to the cases of figure 4. To do that, we substitute for parameters in the obtained expressions for the diffusivity in the two zones by typical values of the southern ocean. The results for the diffusivity and the corresponding eddy kinetic energy are shown in figure 5. As the figure shows, the decay rates of the information away from the interface are very large meaning that $\Im(l)/\Re(l) > 1$ according to figure 4. In fact, $\Im(l)/\Re(l) \sim 40$ for figure 5,.

To investigate if $\Im(l)/\Re(l)$ can be smaller, we set to calculate real and imaginary parts of l. From the dispersion relation we have:

$$l^2 = \frac{\beta k}{(Uk - w) + i\gamma} - k^2 - \kappa_d^2 \tag{70}$$

for $(Uk - w)$ and $k \sim \kappa_d$ we get

$$l^2 = -\frac{i\beta k}{\gamma} - 2k^2 \tag{71}$$

it then can be shown that

$$\Re(l) = k\sqrt{\sqrt{(\frac{\beta}{2k\gamma})^2 + 1} - 1} \tag{72}$$

$$\Im(l) = k\sqrt{\sqrt{(\frac{\beta}{2k\gamma})^2 + 1} + 1} \tag{73}$$

and so

$$\frac{\Im(l)}{\Re(l)} = (\frac{\sqrt{(\frac{\beta}{2k\gamma})^2 + 1} + 1}{\sqrt{(\frac{\beta}{2k\gamma})^2 + 1} - 1})^{\frac{1}{2}}. \tag{74}$$

The fraction $\frac{\Im(l)}{\Re(l)}$ tends to 1 for very large values of $\frac{\beta}{2k\gamma}$ and tends to ∞ for very small values of $\frac{\beta}{2k\gamma}$. So, even for the smallest value of this ratio the interface effects are very limited to the interface neighborhood as shown in case (e) of figure 4. Substituting typical values of the southern ocean in (74) gives a ratio of 40.

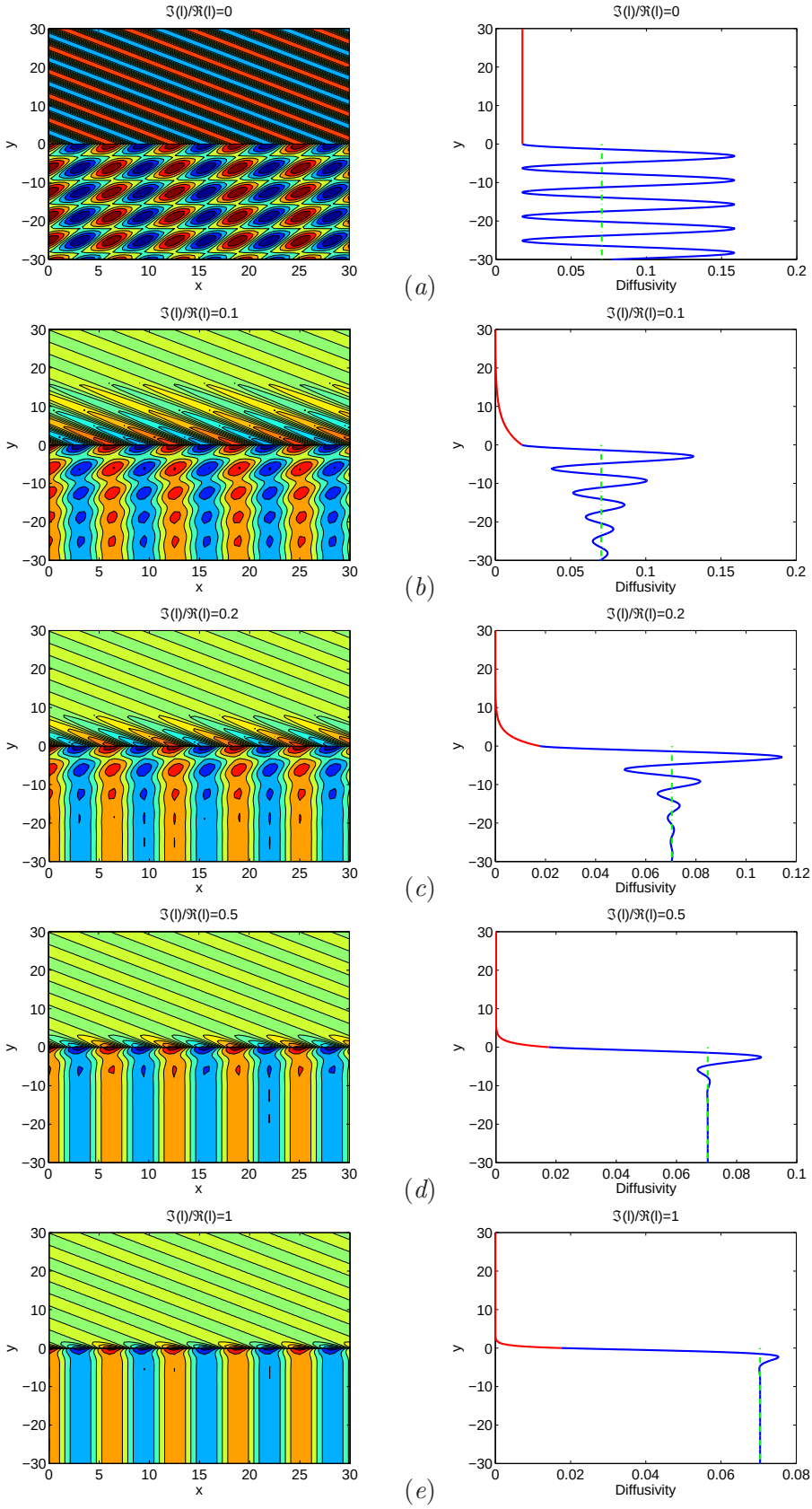

Figure 4: (a) Wave patterns for the intrinsic zero wave velocity in the two zones (left column) and the corresponding effective diffusivity (right column) for $U = 1$, $c_w = U/7$, $k = 1$ and $\Re(l) = 1$. (a) $\Im(l)/\Re(l) = 0$; (b) $\Im(l)/\Re(l) = 0.1$; (c) $\Im(l)/\Re(l) = 0.2$; (d) $\Im(l)/\Re(l) = 0.5$; (e) $\Im(l)/\Re(l) = 1$. Green lines in the right column represent the cons tan diffusivity corresponding to the one-zone problem for the same parameters of each case.

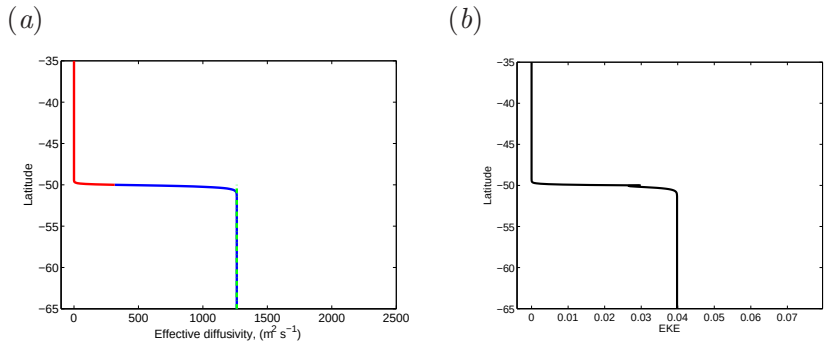

Figure 5: The diffusivity (left) and the corresponding eddy kinetic energy (right) for a case with parameters chosen to be in the range of those of the ACC.

5 Case II: Confined white-noise forcing

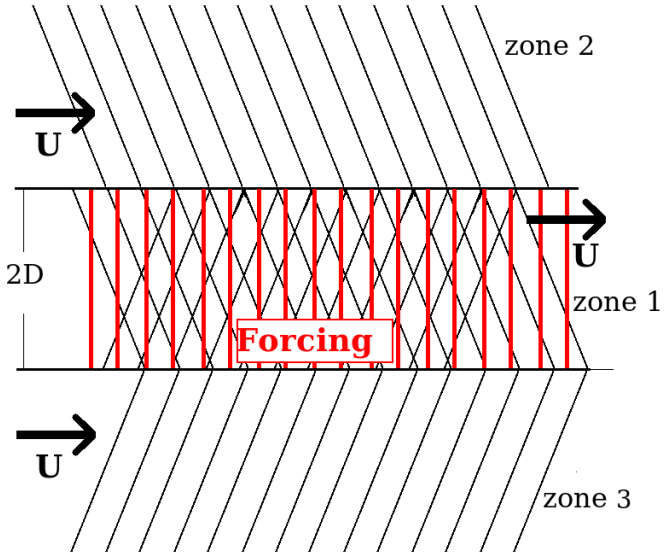

Figure 6: Schematic view of the case II flow configuration.

For the second case with white-noise forcing, we extend the previous case by confining the forcing region into a zone with width $2D$. The flow configuration is shown in figure 6. The velocities are uniform and equal in all three zones. The forcing is only applied to the middle zone (zone 1) and has a form similar to the previous case. The $y = 0$ point is chosen to be half way between the two interfaces in zone 1. As before, the stream functions take

the form

$$\hat{\psi}_1 = (\hat{A}_{1,1}e^{ily} + \hat{A}_{1,2}e^{-ily}) + \hat{\psi}_p, \tag{75}$$

$$\hat{\psi}_2 = \hat{A}_2 e^{ily}, \tag{76}$$

$$\hat{\psi}_3 = \hat{A}_3 e^{-ily}, \tag{77}$$

where ψ_p in zone 1 is similar to the previous case. It should be noted that due to symmetry, both north propagating and south propagating waves are allowed to exist in the middle zone. Applying the first of the jump conditions to the two interfaces gives

$$\begin{aligned} \hat{A}_{1,1}e^{ilD} - \hat{A}_{1,2}e^{-ilD} &= \hat{A}_2 e^{ilD}, \\ \hat{A}_{1,1}e^{-ilD} - \hat{A}_{1,2}e^{ilD} &= -\hat{A}_3 e^{ilD}. \end{aligned} \tag{78}$$

And applying the second jump condition at the two interfaces gives

$$\begin{aligned} \hat{A}_{1,1}e^{ilD} + \hat{A}_{1,2}e^{-ilD} + \hat{\psi}_p &= \hat{A}_2 e^{ilD}, \\ \hat{A}_{1,1}e^{-ilD} + \hat{A}_{1,2}e^{ilD} + \hat{\psi}_p &= \hat{A}_3 e^{ilD}. \end{aligned} \tag{79}$$

And so we get

$$\hat{A}_2 = \hat{A}_3 = -\frac{1}{2}\hat{\psi}_p(e^{ilD} - e^{-ilD}) \tag{80}$$

Considering a tracer equation like before and following the procedure explained in the last case for calculating the flux $< Sv >$ closely, the diffusivities in the three zones become

$$K_1 = \frac{1}{8}\frac{f^2k^2}{\kappa^2}\frac{\gamma}{\gamma^2 + k^2(U - c_w)^2}\,|2 - e^{ilD}(e^{ily} + e^{-ily})|^2, \tag{81}$$

$$K_2 = \frac{1}{8}\frac{f^2k^2}{\kappa^2}\frac{\gamma}{\gamma^2 + k^2(U - c_w)^2}\,|e^{ily}(e^{ilD} - e^{-ilD})|^2, \tag{82}$$

$$K_3 = \frac{1}{8}\frac{f^2k^2}{\kappa^2}\frac{\gamma}{\gamma^2 + k^2(U - c_w)^2}\,|e^{-ily}(e^{ilD} - e^{-ilD})|^2, \tag{83}$$

To demonstrate the variations in the diffusivity expressions obtained for the three zones, figure 7 shows a series of plots similar to those of figure 4. The third zone is not plotted in the figure since it is similar to the second zone but just mirrored with respect to the $y = 0$ line. The green lines in the right column represent the constant diffusivity corresponding to the one-zone problem for the same parameters of each panel. The right panel of the figure shows pure oscillatory motion due to the absence of an imaginary part to l for panel (a). Similar to the previous case, the values of the diffusivity at the interfaces are one fourth of that of the green line. This value retains a constant value in the unforced zone indicating a constant diffusivity. It is important to note that the $\Im(l) = 0$ condition can be achieved only when $\gamma = 0$ which is not permitted as explained before.

As $\Im(l)$ grows larger than zero, the decay in the vertical direction leads to exponential decay of this one-fourth value to zero away from the interface in the upper zone and an oscillatory symmetric pattern in the middle zone forced zone. This can be seen as $\Im(l)$ grows to 0.1 in the case (b). With further increase in $\Im(l)/\Re l$, the decaying layer in each zone

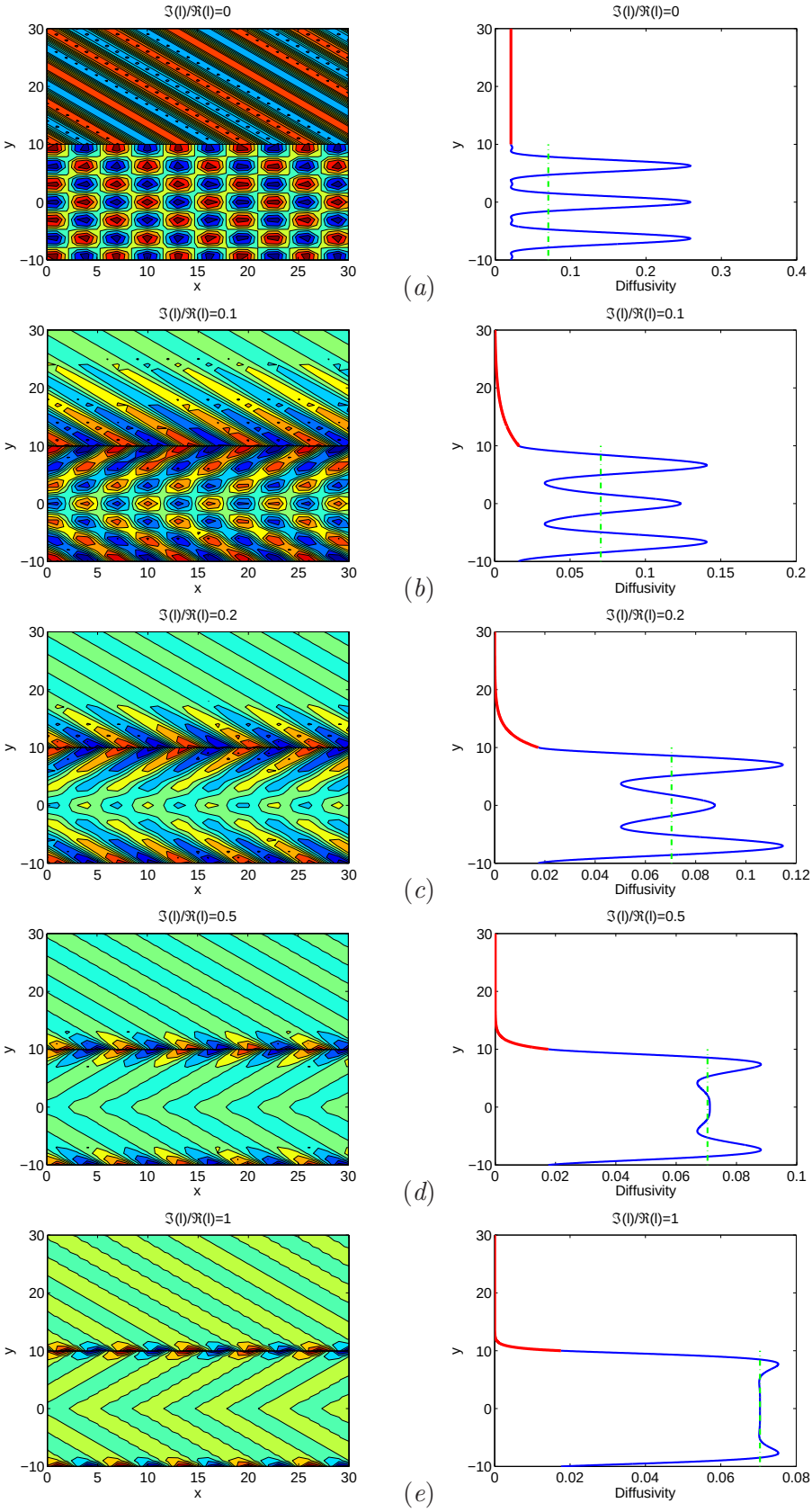

Figure 7: (a) Wave patterns for the intrinsic zero wave velocity in the two zones (left column) and the corresponding effective diffusivity (right column) for $U = 1$, $c_w = U/7$, $k = 1$ and $\Re(l) = 1$. (a) $\Im(l)/\Re(l) = 0$; (b) $\Im(l)/\Re(l) = 0.1$; (c) $\Im(l)/\Re(l) = 0.2$; (d) $\Im(l)/\Re(l) = 0.5$; (e) $\Im(l)/\Re(l) = 1$. Green lines in the right column represent the constant diffusivity corresponding to the one-zone problem for the same parameters of each case.

becomes more compressed about the interface. If we calculate the diffusivity curves for this case using values typical to the southern ocean (similar to figure 5 for the previous case), we find again that the variations in the diffusivities are limited to a very close proximity of the interfaces. And so, The two interfaces will not even feel the effect of each other as if they are each located between two semi-infinite zones.

Comparison of the right column of the figure for larger values of $\Im(l)/\Re l$ (panels (b, c, d)) with figure 7 of FN09 (reproduced in figure 8d in this article) poses some similarities. This may suggest that confinement of the forcing to a zone of a a limited width (2D in our case) can affect the general pattern of the diffusivity in the core of the ACC where the mean velocity is larger than the flanks of the ACC. A close look at figure 2 of FN09 (reproduced in figure 8c in this article) justifies the choice of a confined forcing for this particular patch of the pacific in which we are making the comparisons. As the figure shows, the eddy kinetic energy is dominant in the core of the ACC in the band between 50^oS and 60^oS.

As both figures 4 and 7 showed, the curve for the diffusivity in the unforced zone decay to a small value with a rapid rate, whereas the diffusivity curve in the forced region shows oscillatory behavior. This is mainly due to the absence of the forcing in the top zone. The forcing in the governing equations gives rise to a particular solution from which the oscillatory terms in the diffusivity expressions are originated. So a smoother transition in forcing from the main current to its flanks (zone 1 to zone 2) is needed to capture more variability in the second zone. Also, a change in the velocity from zone 1 to zone 2 might have consequences which can imply more variations in the diffusivity in the unforced zone. The effect of a piece-wise discontinuity in the velocities of the two zones will be briefly visited in the next section.

Regardless of the above arguments however, we have already found out that within the ranges of the parameters associated with the southern ocean all the variations in the diffusivity are compressed to the interface neighborhood. This simply implies that one has to consider smooth variations in the velocity and forcing fields rather than discontinuities considered here. In short, all the interesting physics are compressed into the region of discontinuity by the flow configurations used in our study. However, one can still use the expressions obtained to obtain realistic estimates of the diffusivity from observational data. FN09 described the procedure of translating the observational data into the parameters needed by the expressions we have developed for the diffusivity. Partly (and relatively crudely) following their steps, we can relate the damping rate γ to the eddy kinetic energy through

$$\gamma = d_0^{-1}\sqrt{\kappa^2 EKE}, \tag{84}$$

were d_0 is a constant defined in FN09. We also relate the amplitude of the forcing, f, to the eddy kinetic energy by

$$EKE = \frac{1}{2}f^2, \tag{85}$$

which is not exact for our case but provides a good approximation. We apply these assumptions to the same patch of the pacific ocean as discussed before. The observed EKE for that patch is shown in figure 8(c). To facilitate the calculation, an analytical form if (shown in panel a) is fitted to the EKE curve in panel c. There are few other parameters

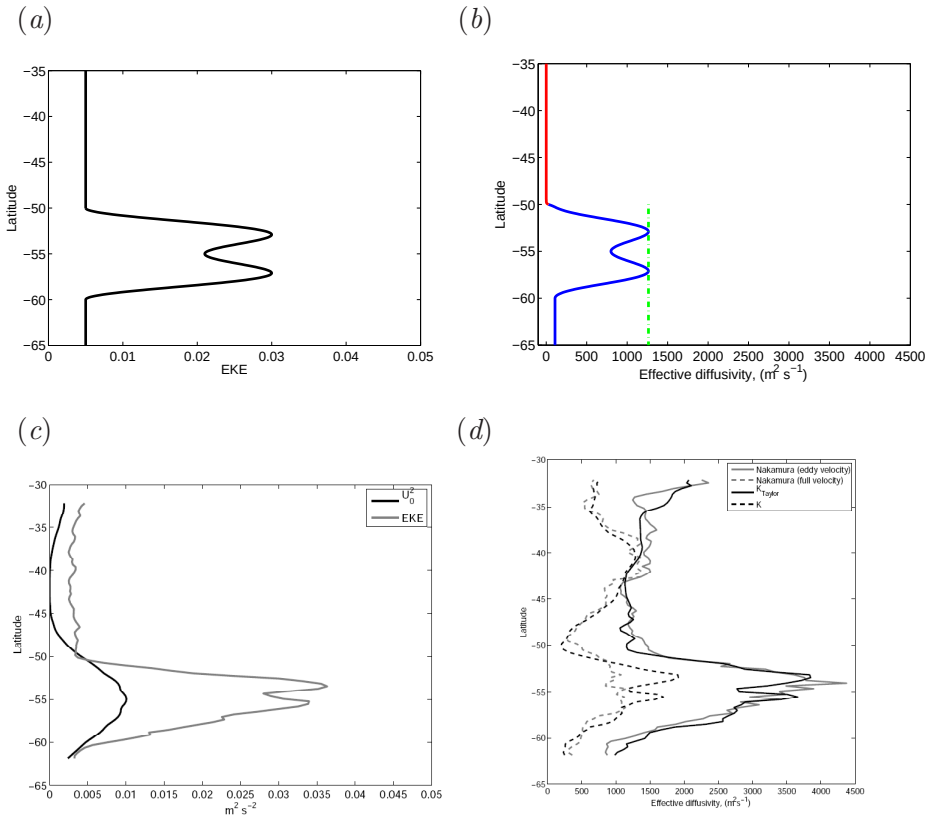

Figure 8: (a) An analytical fit to the observational EKE (shown in panel (c)) used in the present model; (b) Calculated diffusivity corresponding to the EKE of panel (a); (c) Zonally averaged eddy kinetic energy EKE in gray for a patch in the pacific sector of the Southern Ocean; (d) Diffusivities calculated by using various methods. (c,d) are from Ferrari and Nikurashin(2009)

.

needed to be determined for calculating the diffusivity from (81,82). The y-wavenumber, l, can be obtained from the dispersion relation (47) by setting $\omega = U_i k$ for each case. The x-wavenumber k is set to be that of the most unstable mode of the baroclinic instability and a typical value for the southern ocean is used for the deformation radius. Plugging these information into (81,82) we obtain the curves for diffusivities in the two regions. The curves are shown in the panel (b) of figure 8. The green line is defined similar to figures 4 and 7. Comparing the result with those predicted by FN09 (dashed lines in panel (d) of our figure 8), it seems that our calculation captures the size and pattern reasonably well. Indeed, all that we have achieved is to map the EKE map of panel (a) into the diffusivity curve of panel (b) through the parameters γ and f. And hence, there is not much variation in our diffusivity curve in the unforced zone because of the very small constant value of EKE considered in that zone. One can wonder how come the EKE curve of panel (c) leads to the diffusivity curves of panel (d) whereas that is not the case in our calculations

from (a) to (b). Probably the answer is that some physical phenomena accruing in the flanks are being missed out of our modeling due to our flow configurations. This will be further discussed in the discussion section.

6 Case III: Semi-infinite forcing with discontinuous velocity

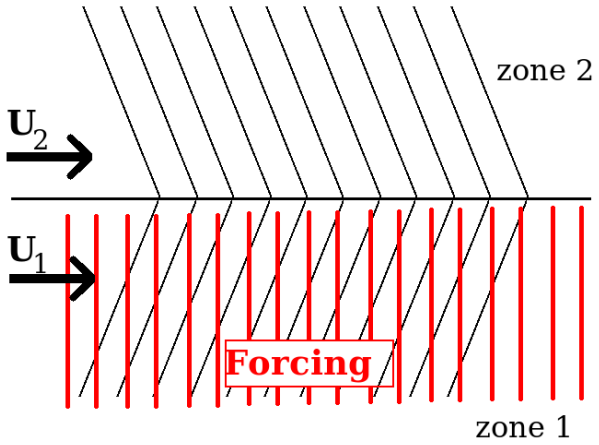

Figure 9: Schematic view of the case III flow configuration.

As the last case in this study, we also allow for a piecewise discontinuity in the velocity field (unlike the previous two cases) with white-noise forcing. Although previous cases have taught us that we should expect the consequences of the velocity discontinuity to be confined to the close neighborhood of the interface, this case might give some insight into possible outcomes of a change in the jet velocity. The flow configuration is schematically shown in figure 9. As previous cases, we start by writing the general form of the stream functions in the two regions

$$\hat{\psi}_1 = \hat{A}_1 e^{il_1 y} + \hat{\psi}_p, \tag{86}$$

$$\hat{\psi}_2 = \hat{A}_2 e^{il_2 y}. \tag{87}$$

It should be noted that the y-wavenumber components $l_1(\omega), l_2(\omega)$ are not the same anymore due to the velocity discontinuity. The jump conditions for this case become

$$l_2(\omega + U_1 k)(k^2 + l_1^2)\hat{A}_1 = l_1(\omega + U_2 k)(k^2 + l_2^2)\hat{A}_2, \tag{88}$$

$$(\omega + U_2 k)(\hat{A}_1 + \hat{\psi}) = (\omega + U_1 k)\hat{A}_2. \tag{89}$$

Solving for $\hat{A}_1$ and $\hat{A}_2$ we get

$$\hat{A}_1(\omega) = \frac{l_1(\omega + U_2 k)^2(k^2 + l_2^2)}{l_2(\omega + U_1 k)^2(k^2 + l_1^2) - l_1(\omega + U_2 k)^2(k^2 + l_2^2)}\hat{\psi}_p \tag{90}$$

$$\hat{A}_2(\omega) = \frac{l_2(\omega + U_1 k)(\omega + U_2 k)(k^2 + l_1^2)}{l_2(\omega + U_1 k)^2(k^2 + l_1^2) - l_1(\omega + U_2 k)^2(k^2 + l_2^2)}\hat{\psi}_p \tag{91}$$

In the case of $U_1 = U_2$, we have $l_1 = -l_2$ and these jump conditions reduce to (55, 56) obtained for Case I. The stream functions become

$$\hat{\psi}_1 = (\tilde{A}_1 e^{il_1 y} + 1)\hat{\psi}_p, \tag{92}$$

$$\hat{\psi}_2 = \tilde{A}_2 e^{il_2 y}\hat{\psi}_p, \tag{93}$$

where $\tilde{A}_1$ and $\tilde{A}_2$ are the fractions on the right hand sides of (90, 91) respectively. Finally, the expressions for the diffusivity in the two regions take the form

$$K_1 = \frac{1}{2}\frac{f^2k^2}{\kappa^2}\frac{\gamma}{\gamma^2 + k^2(U_1 - c_w)^2}\ |\tilde{A}_1 e^{il_1 y} + 1|^2_{(at\ U_1 k)}, \tag{94}$$

$$K_2 = \frac{1}{2}\frac{f^2k^2}{\kappa^2}\frac{\gamma}{\gamma^2 + k^2(U_2 - c_w)^2}|\tilde{A}_2 k e^{il_2 y}|^2_{(at\ U_2 k)}, \tag{95}$$

where the subscripts $(at\ U_i k)$ imply that the expressions should be evaluated at $\omega = U_i k$ for each case. Two points can be pointed out by looking at (94,95). First, similar to previous cases the expression for K_2 decays exponentially in zone 2 while the $|\tilde{A}_1 e^{il_1 y} + 1|^2$ term in (94) allows for oscillatory behavior in the forced zone. Second point is that one might argue that only the difference between the two velocities U_1 and U_2 matters as one can move with the reference frame attached to one of the zones and hence set its velocity to zero. However, that is not possible due to the dependence of the diffusivities in the two zones on the $(U_1 - c_w)$ and $(U_2 - c_w)$ terms. So it is the difference of the velocity of the main flow and the eddy propagation velocity that really matters for mixing in each zone.

Figure 10 shows the diffusivity curves in the two zones for different U_2/U_1 ratios. The plots are made for typical values for the southern ocean similar to figure 5. It should be noted that the figures (5, 10) differ from figure 8 in that fixed values for EKE (and subsequently fixed values of γ and f) are used in obtaining them. The velocity of zone 1 is chosen to be 15 cm/s and c_w is taken to be $U1/7$. The first panel simply recovers the results of case I as the velocity ratio is unity. However, the value of the diffusivity at the interface is changed as the velocity ratio is varied. This is shown by the overlapping of the blue and red curves in panel (b) and the discontinuity between them in panel (c). So, the unphysical sharp discontinuity in the velocity field leads to an expected unphysical discontinuity in the diffusivity. It should also be noted that the value of the diffusivity on each side of the interface does not show a monotonic behavior with the change in the velocity ratio. This can be clearly seen by comparing the tips of the red and blue lines at the interface and comparing them for the three cases in the figure. As before, the fast decay of the information away from the interface emphasizes the necessity of considering smoother changes in the velocity and forcing fields.

7 Conclusion

The aim of this project was to investigate the effects of variations in the forcing and the velocity field employed in the FN09 model on the expression for the diffusivity. Several test cases where considered with piecewise discontinuities in both the forcing and the velocity fields. It was shown mathematically that among the numerous radiative waves produced

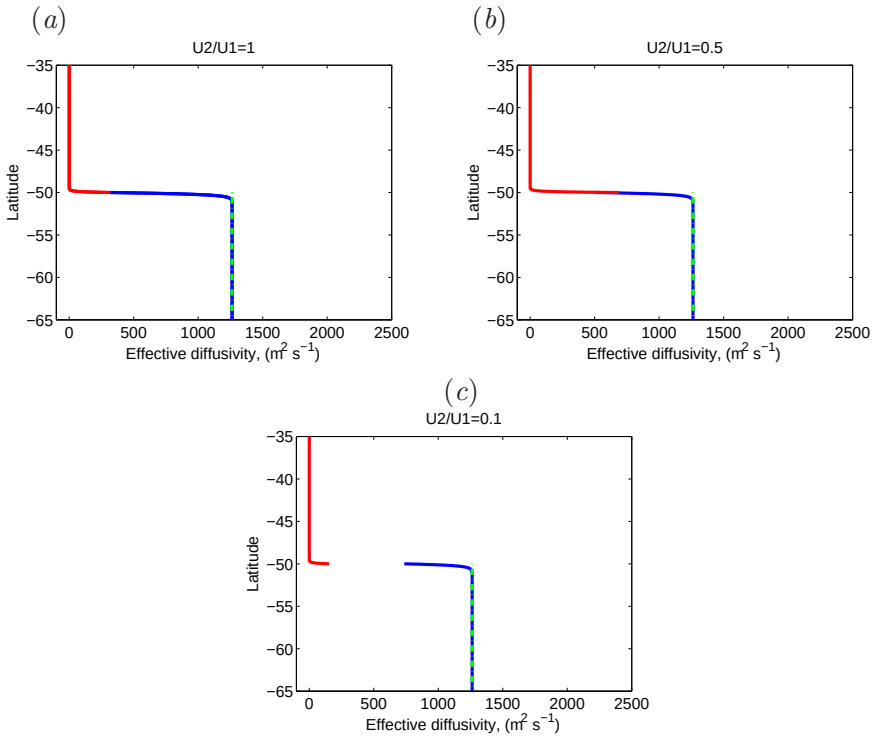

Figure 10: The diffusivity for three cases with different velocity rations. (a) $U_2/U_1 = 1$; (b) $U_2/U_1 = 0.5$; (c) $U_2/U_1 = 0.1$. The parameters are chosen in a similar way to figure 5.

through the discontinuity at the interface, only the one with a phase speed equal to the ambient jet velocity is the one contributing to the mixing process. This finding is of a great physical importance and also provides a very efficient tool for calculating the diffusivities. The mathematical derivations would be more rigorous without this finding. The results of this study suggest that one needs to consider a smoother variation in the velocity field to obtain more information about the mixing in the flanks of the jet. An estimate for the meridional variations in the velocity field can be obtained from the observational data such as those presented in FN09 both for the pacific patch and for the zonally averaged case. Considering a smoothly varying jet velocity enables investigating the presence of the critical layers in the flanks of the ACC and their implications for the mixing. As an instructional example, one can simply apply the expression derived for the eddy diffusivity in FN09 (equation (6) in this article) to a jet with a zonal velocity which uniformly decreases with y. By keeping the other parameters constant (for the sake of physical intuition), the denominator of the expression for the flux becomes smaller as the jet velocity is reduced as the $(U - c_w)$ becomes smaller. At a critical layer where the jet velocity reaches the speed of propagation of the eddies, the diffusivity obtains a maximum value. Although this argument is only true as long as the other parameters are kept constant, it shows that one can expect a rise in the eddy diffusivity in the regions where the jet velocity has reduced to a value close to c_w. The enhancing effect of the critical layers was suggested by Marshal *et al.*(2006) [3]

and seems to be in agreement with the results of FN09. The introduction of a continuously varying jet velocity into the governing equations may pose analytical difficulties but one might be able to choose a profile which makes the mathematical derivations easier (such as the work of Talley (1983) [5]).

Another important feature of all the results of our study was the fast decay of the effects of the interface away from it. By revisiting the procedure we followed in the stability analysis, we note that the solutions were sought in the form of $e^{i(kx-ct)}$, where c was assumed real. This assumption was made to exclude the temporally growing modes. However, the final results indicated a fast spacial decay (and so "trapped" waves). One can wonder if there might be modes that can grow in time but decay in space? Indeed stability analysis done with allowance for a complex c (and thus the possibility of growing modes) shows that those modes can exist. They might grow in time and decay in space (in the y direction) in a way that they form a wave-packet travelling north (or south) with a group velocity. Or, they might still be trapped but decay to zero much slower than our results (due to their temporal growth). Either way, these waves can propagate information much further from the interface compared to our results. A nice discussion on these groups of waves can be found in Kamenkovich and Pedlosky (1995) [2].

So, it seems that the first step in extending this study is to revisit the cases considered in this work by allowing for modes with temporal growth rates which were not included. This can allow for the information to propagate further from the interface which can have interesting implications for the mixing in the flanks of the jet. Allowing for continuous variations in the velocity would also be a natural step towards building a more realistic model.

In the end, I would like to thank

Both my advisers for all the time they spent with me on this project,
Joe Pedlosky for the instructive discussions we had,
The GFD program for accepting me as a fellow,
George Veronis for the softball experience,
Marco for being such a nice roommate and helping me out in the world of vegetable,
The 2009 fellows for the fun experience,
and
All the GFD staff for helping such a wonderful program to exist.

References

[1] R. Ferrari and M. Nikurashin, *Suppression of eddy diffusivity across jets in the southern ocean*, submitted to J. Phys. Oceanogr., (2009).

[2] I. Kamenkovich and J. Pedlosky, *Radiating instability of nonzonal ocean currents*, J. Phys. Oceanogr., (1995).

[3] J. Marshall, E. Shuckburgh, H. Jones, and C. Hill, *Estimates and implications of surface eddy diffusivity in the southern ocean derived from tracer transport*, J. Phys. Oceanogr., (2006).

[4] L. Rayleigh, *On the stability or instability of certain fluid motions.*, Scientific Papers, Vol.1, 474-487, (1980).

[5] L. Talley, *Radiating barotropic instability*, J. Phys. Oceanogr., (1983).

8 Appendix A

The second jump condition can be obtained by setting the solution for the interface perturbation η obtained in the two zones to be equal to each other. The interface perturbation η is shown schematically in figure 11. The equations for η in the two zones have the form

$$\frac{D\,\eta}{D\,t} = \partial_t \eta + U_1 \partial_x \eta = v_1 = -\partial_x \psi_1 \tag{96}$$

$$\frac{D\,\eta}{D\,t} = \partial_t \eta + U_2 \partial_x \eta = v_2 = -\partial_x \psi_2 \tag{97}$$

Taking the Fourier transform of the two equations and expecting η to have the same x-dependence as the stream functions (i.e., e^{ikx}), we get

$$\partial_t \hat{\eta} + ikU_1 \hat{\eta} = ik\hat{\psi}_1 \tag{98}$$

$$\partial_t \hat{\eta} + ikU_2 \hat{\eta} = ik\hat{\psi}_1 \tag{99}$$

Subtracting (99) from (98) we get

$$\hat{\eta} = \frac{\hat{\psi}_1 - \hat{\psi}_2}{U_1 - U2}. \tag{100}$$

substituting (100) into (98) gives the jump condition

$$(\partial_t + ikU_1)(\hat{\psi}_1 - \hat{\psi}_2) = ik\hat{\psi}_1(U_1 - U_2). \tag{101}$$

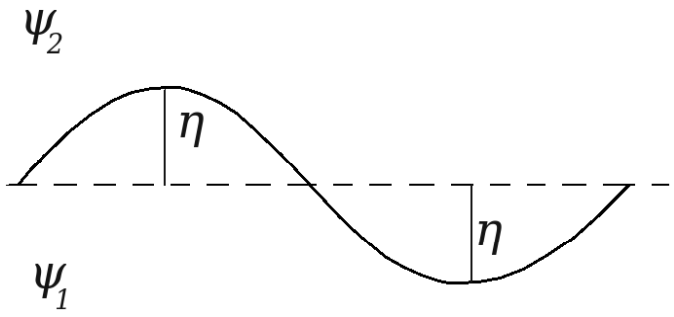

Figure 11: Schematic view of the perturbation of the interface between zones 1 and 2.

9 Appendix B

The goal of this appendix is to to show that **if** two complex functions $S(t)$ and $V(t)$ satisfy the relations

$$S_t = V(t), \tag{102}$$
$$V(t) = A(t) * r(t), \tag{103}$$

where $A(t)$ is a general function and $r(t)$ satisfies

$$C(t-t') =< r(t)r(t')^* >= a\ stationary\ function, \tag{104}$$

then the following is true:

$$< Sv >= \frac{1}{2}|\hat{A}(0)|^2 C(0). \tag{105}$$

C is the covariance function and '*' denotes the convolution of the two functions. The fact that $C(t-t')$ is stationary means that it only depends on $\Delta t = t - t'$ and not on t or t'. To start the proof we have

$$< Sv >= \frac{1}{2}\frac{d}{dt} < S^2 >= \frac{1}{2}\int_0^t < V^*(t)V(t') > dt' = \frac{1}{2}\int_{-\infty}^{\infty} < V^*(t)V(t-t') > dt'. \tag{106}$$

Its easy to show that the second and term expressions are equal in the above equality. The integrand in the last expression in (106) can be simplified to

$$\begin{aligned} &< V^*(t)V(t-t') >=< (A*r)^*|_t (A*r)|_{t-t'} >= \\ &< \int_{-\infty}^{\infty}\int_{-\infty}^{\infty} A^*(t-t_1)r^*(t_1)A(t-t'-t_2)r(t_2)dt_1dt_2 >= \\ &\int_{-\infty}^{\infty}\int_{-\infty}^{\infty} A^*(t-t_1)r^*(t_1)A(t-t'-t_2)C(t_1-t_2)dt_1dt_2, \end{aligned} \tag{107}$$

where C is defined in (104). Replacing the last expression back into (106) and integrating with respect to t' we get

$$< Sv >= \frac{1}{2}\hat{A}(0)\int_{-\infty}^{\infty}\int_{-\infty}^{\infty} A^*(t-t_1)C(t_1-t_2)dt_1dt_2.$$

Next integrating with respect to t_2 we get

$$< Sv >= \frac{1}{2}\hat{A}(0)\hat{C}(0)\int_{-\infty}^{\infty} A^*(t-t_1)dt_1.$$

And finally integrating with respect to t_1 we get

$$< Sv >= \frac{1}{2}\hat{A}(0)\hat{A}^*(0)\hat{C}(0) = \frac{1}{2}|\hat{A}(0)|^2\hat{C}(0). \tag{108}$$

This completes the proof. Had we included a constant b in the definition of $V(t)$ at the beginning (i.e., $V(t) = bA(t) * r(t)$), the final result (108) would become

$$< Sv >= \frac{1}{2}|bb^*||\hat{A}(0)|^2\hat{C}(0). \tag{109}$$

For a white noise function $r(t)$ (used throughout this article) we get

$$C(t-t') =< r(t)r(t')^* >= \delta(t-t'),$$

and so

$$\hat{C}(0) = 1. \tag{110}$$